SIAM J. APPL. MATH.
Vol. 72, No. 1, pp. 201–215
© 2012 Society for Industrial and Applied Mathematics

AN ASYMPTOTIC THEORY FOR THE RE-EQUILIBRATION OF A MICELLAR SURFACTANT SOLUTION*

I. M. GRIFFITHS†, C. D. BAIN‡, C. J. W. BREWARD†, S. J. CHAPMAN†, P. D. HOWELL†, AND S. L. WATERS†

Abstract. Micellar surfactant solutions are characterized by a distribution of aggregates made up predominantly of premicellar aggregates (monomers, dimers, trimers, etc.) and a region of proper micelles close to the peak aggregation number, connected by an intermediate region containing a very low concentration of aggregates. Such a distribution gives rise to a distinct two-timescale re-equilibration following a system dilution, known as the τ_1 and τ_2 processes, whose dynamics may be described by the Becker–Döring equations. We use a continuum version of these equations to develop a reduced asymptotic description that elucidates the behavior during each of these processes.

Key words. Becker–Döring equations, surfactant systems, micellar kinetics, asymptotic analysis

AMS subject classifications. 45K05, 82C70, 35Q99

DOI. 10.1137/110842089

1. Introduction.

1.1. Micellar reaction kinetics. When surfactant exceeds a particular bulk concentration in solution, termed the *critical micelle concentration* (CMC), it becomes favorable for aggregates or *micelles* to form. The micelles can have various sizes and shapes, but for many simple surfactants with a single hydrocarbon chain the aggregates are approximately spherical and contain of the order of 100 monomers [11]. The distribution of aggregate sizes is localized around this optimum value with a half-width of the order of the square root of the aggregation number. Aggregates that are much smaller than the mean aggregation number are energetically highly unfavorable and consequently appear in much lower concentrations [1, 2, 3, 13].

The re-equilibration and subsequent restructuring of a micellar surfactant solution upon a disturbance from equilibrium is of great importance for the adsorption kinetics of micellar solutions. The coagulation and breakdown of micellar aggregates in a surfactant system is generally assumed to occur via stepwise monomer loss or gain [1, 2, 3, 7], which may be expressed via the following series of reactions:

$$\text{monomer} + n\text{-mer} \underset{\kappa_n^-}{\overset{\kappa_n^+}{\rightleftharpoons}} (n+1)\text{-mer}, \tag{1.1}$$

where the term n-mer denotes an aggregate containing n monomers, and $\kappa_n^{\pm}$ are the association and dissociation rate coefficients. The reaction kinetics for this system are

*Received by the editors July 22, 2011; accepted for publication (in revised form) November 17, 2011; published electronically January 24, 2012. This work was supported by Award KUK-C1-013-04, made by King Abdullah University of Science and Technology (KAUST), and by EPSRC grant EP/E019323.

http://www.siam.org/journals/siap/72-1/84208.html

†Mathematical Institute, University of Oxford, 24-29 St. Giles', Oxford, OX1 3LB, UK (ian.griffiths@maths.ox.ac.uk, breward@maths.ox.ac.uk, chapman@maths.ox.ac.uk, howell@maths.ox.ac.uk, waters@maths.ox.ac.uk). The fifth author is grateful to the EPSRC for funding in the form of an Advanced Research Fellowship.

‡Department of Chemistry, Durham University, Durham, DH1 3LE, UK (c.d.bain@durham.ac.uk).

Copyright © by SIAM. Unauthorized reproduction of this article is prohibited.

described by the *Becker–Döring* equations [4]

$$\frac{\mathrm{d}\mathcal{X}_n}{\mathrm{d}\mathcal{T}} = \kappa^+_{n-1}\mathcal{X}_1\mathcal{X}_{n-1} - \kappa^-_{n-1}\mathcal{X}_n - \kappa^+_n\mathcal{X}_1\mathcal{X}_n + \kappa^-_n\mathcal{X}_{n+1} \tag{1.2}$$

for $n \geq 2$, where $\mathcal{X}_n = \mathcal{X}_n(\mathcal{T})$ denotes the (molar) concentration of an aggregate containing n monomers at time $\mathcal{T}$.

The net bulk concentration of monomers contained in all aggregates is given by

$$\mathcal{C}_b = \sum_{n=1}^{\infty} n\mathcal{X}_n, \tag{1.3}$$

so that, under the assumption that $\mathcal{C}_b$ is conserved for all time, the free monomer concentration is determined by

$$\mathcal{X}_1(t) = \mathcal{C}_b - \sum_{n=2}^{\infty} n\mathcal{X}_n(t) = \mathcal{X}_1(0) - \sum_{n=2}^{\infty} n\big(\mathcal{X}_n(t) - \mathcal{X}_n(0)\big). \tag{1.4}$$

Along with (1.2), this gives us an infinite-dimensional system of ODEs for $\mathcal{X}_2(t), \mathcal{X}_3(t), \ldots$. The solution of this system requires us to specify all the initial concentrations $\mathcal{X}_1(0), \mathcal{X}_2(0), \ldots$, and the association and dissociation rate coefficients, $\kappa^{\pm}_n$.

The Becker–Döring system of equations is commonly used to consider systems in which the monomer concentration is held constant or deviates only slightly from equilibrium, or in which the aggregates are assumed to have a uniform concentration distribution, simplifying the analysis significantly. However, the re-equilibration of a surfactant with a realistic aggregate distribution, following an order-one dilution, is much less well studied. As a consequence, there exist many applications of the theories for small deviations in monomer concentration (e.g., [1, 2, 3]) to situations where the deviations from equilibrium are much too large for the theory to be applicable.

The full Becker–Döring model is used to investigate the relaxation, following an order-one dilution (which leaves the system above the CMC), of a micellar surfactant solution with a realistic equilibrium aggregate distribution in [7]. (The key results of this paper are summarized in Appendix A.) In this case, the monomer concentration must be replenished to its equilibrium value via the breakdown of some of the aggregates, while a proportion of surfactant will still reside in aggregate form.

The re-equilibration process following dilution occurs in two distinct stages which are inherently related to the shape of the aggregate distribution [7, 9]. First, aggregates shed individual monomers which replenish the concentration of monomers. This is called the τ_1 process [1, 2, 3, 7]. However, since the stability of aggregates falls rapidly with decreasing aggregation number, this process becomes energetically unfeasible before it has supplied enough material to replenish the monomer to its new equilibrium value. As a result, some of the aggregates have to break down completely to replenish the monomer fully to the new equilibrium. The remaining monomers associate with those aggregates which have not broken down, increasing the typical aggregation number and hence their stability. This second process is called the τ_2 process [1, 2, 3, 7]. The τ_2 process is governed by the rate at which micelles are able to break down entirely, which is set by the concentration of aggregates in the intermediate region of aggregates that lie between monomers and proper micelles: the lower the concentration of aggregates, the longer the time taken to re-equilibrate. Thus, for

Copyright © by SIAM. Unauthorized reproduction of this article is prohibited.

typical surfactant systems with an extremely low concentration of intermediate aggregates, this leads to an extreme separation of timescales for the τ_1 and τ_2 processes. In this paper we employ an asymptotic theory to provide simplified models for the detailed behavior during each of these processes.

This paper is structured as follows. In section 2 we outline the fundamental mathematical model, determine the reaction rates along with the initial and equilibrium distributions, and detail the continuum system of equations and boundary conditions that govern the re-equilibration behavior. In section 3 we develop reduced models for each of the two stages of re-equilibrium. We conclude by discussing the application of these models to enhance the understanding of micellar reaction kinetics.

2. The mathematical model.

2.1. Determining the reaction rates. Ultrasonic adsorption studies [15, 16] suggest that reactions proceed at a diffusion-controlled rate, so that

$$\kappa_n^+ = 4\pi N_A \sigma_n \left(D_1 + D_n\right), \tag{2.1}$$

where N_A is the Avogadro number, D_n represents the diffusion coefficient of an aggregate of size n, and σ_n is the collision radius. We may take σ_n to be the sum of the aggregate radii, $r_1 + r_n$ (with r_n proportional to $n^{1/3}$), and the Stokes–Einstein equation provides a relation between the diffusion coefficient of an aggregate and its size, namely

$$D_n = \frac{k_B T}{6\pi\eta r_n}, \tag{2.2}$$

where k_B is the Boltzmann constant, and T and η are the temperature and viscosity of the solution. This provides the estimate

$$\kappa_n^+ = \left(\frac{2k_B N_A T}{3\eta}\right) \frac{\left(1 + n^{1/3}\right)^2}{n^{1/3}}, \tag{2.3}$$

which gives $\kappa_1^+ \sim 10^6\,\mathrm{m^3\,mol^{-1}\,s^{-1}}$ for a surfactant in water at 300K. Such reaction rates are in line with spectroscopic stopped-flow experiments on the polyoxyethylene glycol alkyl ether surfactant C_nE_m series, where rapid re-equilibration is observed to occur before data acquisition begins, that is, on a timescale less than 10 ms [5]. The estimate (2.3) predicts rather weak dependence of the association rates upon aggregate size: for example, κ_{200}^+ is roughly twice κ_1^+. As a first approximation we therefore suppose henceforth in this paper that the association rates are all equal. (Further numerical studies show that the generic system behavior observed is not significantly affected by allowing the association rates to vary with aggregate size.)

The dissociation rates κ_n^- are not well characterized, but we may determine these if we know the equilibrium distribution, say $\mathcal{X}_n = \mathcal{X}_n^*$ by the following method. At equilibrium, the principle of microscopic reversibility requires that each mechanistic step in a reversible reaction must itself be in equilibrium, and so, from (1.2), we must have

$$\kappa_n^+ \mathcal{X}_1^* \mathcal{X}_n^* = \kappa_n^- \mathcal{X}_{n+1}^*, \tag{2.4}$$

which may be rearranged to provide an expression for the dissociation rates in terms of the association rates and equilibrium distribution,

$$\kappa_n^- = \left(\frac{\mathcal{X}_1^* \mathcal{X}_n^*}{\mathcal{X}_{n+1}^*}\right) \kappa_n^+ \tag{2.5}$$

for $n \geq 1$.

Copyright © by SIAM. Unauthorized reproduction of this article is prohibited.

2.2. The equilibrium distribution. Determination of the equilibrium size distribution, $\mathcal{X}_n^*$, for different surfactants and different micelle shapes is a subject of extensive debate. Since concentrations in the intermediate aggregate region are orders of magnitude smaller than those close to the optimum aggregation number, there are no direct experimental methods available for their measurement. It is, however, possible to calculate an equilibrium aggregate size distribution from knowledge of the chemical potential differences between monomers in different sized aggregates. This may be done via Molecular Dynamics (MD) simulations [6, 8, 10] or by Molecular Thermodynamics (MT) [12, 13, 14].

The standard chemical potential for an aggregate of size n, μ_n, is related to the size distribution X_n via

$$\mu_n + k_B T \log(X_n) = n\left(\mu_1 + k_B T \log(X_1)\right), \tag{2.6}$$

which may be rearranged to give the size distribution,

$$X_n = X_1^n \exp\left(-\frac{n}{k_B T}\left(\frac{\mu_n}{n} - \mu_1\right)\right). \tag{2.7}$$

The shape of the aggregate distribution is governed by the precise functional form of μ_n, which is made up of contributions resulting from the transfer and deformation free energy of the surfactant tail, the aggregate core–water interfacial free energy, and head group steric interactions and deformation (see [13] for further details).

Both MD and MT methods predict a distribution characterized by the following key features. Almost all surfactant material is contained within either a region of *premicellar aggregates* (monomer, dimers, trimers, etc.) or a region of *proper micelles* close to the peak aggregation number, which is typically large. These are connected by an *intermediate region* containing a very low concentration of aggregates; see Figure 2.1.

It was shown in [7] that the important behavior of the system may be captured by approximating the distribution as

$$\frac{\mathcal{X}_n^*}{\mathcal{X}_1^*} = \begin{cases} 1, & n = 1, \\ \dfrac{B}{m^{3/2}} \exp\left(-\beta m\left(n/m - 1\right)^2\right) + \dfrac{C}{m^2}\exp(-dn/m), & n \geq 2, \end{cases} \tag{2.8}$$

where $B \approx 2.26$, $\beta \approx 0.76$, $m = 70$, $C \approx 5 \times 10^{-9}$, and $d \approx 15$ are parameters determined by fitting to an MT simulation as shown in Figure 2.1. This captures the distribution of proper micelles with a width determined by β and the spike at $n = 1$. The dependence of the prefactors of the second and third terms in (2.8) on the optimal aggregation number is shown explicitly as a premultiplication by $1/m^{3/2}$ and $1/m^2$, respectively; B and C are assumed to be independent of m. The largeness of m ensures the high relative concentration of monomer to aggregates, as well as a narrow Gaussian spread around $n = m$. The relative concentration of intermediate aggregates for a typical surfactant, set by the parameters C and d, is generally extremely low, and this is highlighted by the smallness of C.

2.3. The postdilution distribution. Since $m \equiv 1/\epsilon$ is typically large, the distribution (2.8) is appropriately represented by a continuum function for the aggregate concentrations (becoming exact in the limit $\epsilon \to 0$). We thus let $x = n/m$ and define the continuum order-one function $Y(n/m) = m^2 \mathcal{X}_n^*/\mathcal{X}_1^*$ for $n \geq 1$, and we treat the

Copyright © by SIAM. Unauthorized reproduction of this article is prohibited.

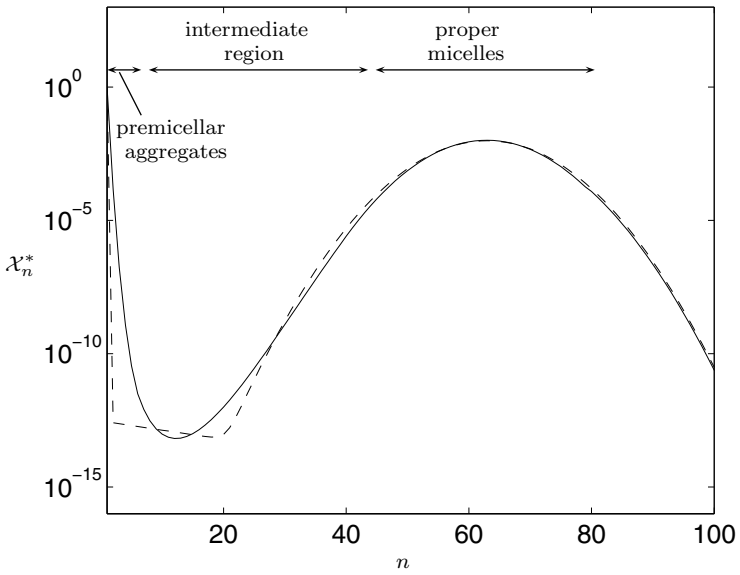

FIG. 2.1. *An equilibrium aggregate size distribution predicted by MD simulation for the polyoxyethylene glycol alkyl ether surfactant $C_{10}E_8$ at a bulk concentration $C_b = 10\,mM$ (solid line)* [5]. *The dashed line shows the approximation* (2.8)*, with $A = 1$, $b = 7$, $B \approx 4.82$, $\beta \approx 0.9$, $m = 63$, $C \approx 3 \times 10^{-13}$, $d \approx 5$.*

monomer concentration separately (see [7] for details). The prefactor m^2 is chosen to ensure that Y is an order-one function when the proportion of surfactant in aggregate form is comparable with the concentration in monomer form. In addition, since C is typically extremely small for realistic surfactant systems (as shown in Figure 2.1) we henceforth choose to study the re-equilibration for profiles where $C = 0$. Thus

$$Y = \frac{B}{\sqrt{\epsilon}} \exp\left(-\frac{\beta}{\epsilon}(x-1)^2\right). \tag{2.9}$$

We then dilute by a factor of D and analyze the evolution of the resulting distribution to the new equilibrium. For simplicity we choose to scale all concentrations in the subsequent analysis with the postdilution equilibrium monomer concentration. The initial distribution instantaneously after dilution, $y_0(x)$, and the new equilibrium distribution, $\overline{y}(x)$, are then given by [7]

$$y_0(x) = y(x,0) = \frac{Y(x)}{\nu D} = \frac{B_0}{\sqrt{\epsilon}} \exp\left(-\frac{\beta}{\epsilon}(x-1)^2\right), \tag{2.10a}$$

$$\overline{y}(x) = \lim_{t\to\infty} y(x,t) = Y(x)\nu^{x/\epsilon - 1} = \frac{\overline{B}}{\sqrt{\epsilon}} \exp\left(-\frac{\beta}{\epsilon}(x-\overline{\omega})^2\right), \tag{2.10b}$$

while the corresponding monomer concentrations are

$$X_1(0) = \frac{1}{\nu D}, \qquad \lim_{t\to\infty} X_1(t) = \overline{X}_1 = 1. \tag{2.10c}$$

Here the parameter ν corresponds to the ratio of the equilibrium monomer concentration following dilution to the original equilibrium monomer concentration and is

Copyright © by SIAM. Unauthorized reproduction of this article is prohibited.

determined via the expression for conservation of mass for a given dilution:

$$1 + \int_0^\infty x\overline{y}(x)\,\mathrm{d}x = \frac{C_b}{\nu D}, \tag{2.11}$$

where C_b is the dimensionless predilution bulk concentration scaled with $\mathcal{X}_1^*$. This parameter arises as a consequence of our choice of nondimensionalization to ensure that the dimensionless equilibrium monomer concentration following dilution is equal to 1. Provided the system remains micellar, ν is typically close to (but slightly less than) unity. This reflects the fact that the monomer concentration is approximately constant (and equal to the CMC) for any given bulk concentration when the system is in micellar form: above this bulk concentration, micelles are typically able to form. The remaining parameters in (2.10) are related to the predilution distribution by

$$B_0 = \frac{B}{\nu D}, \qquad \overline{B} = B\nu^{1/\epsilon - 1}\exp\left(\frac{\log^2\nu}{4\epsilon\beta}\right), \qquad \overline{\varpi} = 1 + \frac{\log\nu}{2\beta}, \qquad \overline{\beta} = \overline{\varpi}\beta. \tag{2.12}$$

Substituting for $\overline{y}$ using (2.10b) allows us to evaluate the integral in (2.11) explicitly to give

$$\frac{C_b}{D} - \nu = B\sqrt{\frac{\pi}{\beta}}\,\overline{\varpi}\mathrm{e}^{-\beta m(1-\overline{\varpi})^2} G\left(\overline{\varpi}\sqrt{\beta m}\right), \tag{2.13}$$

where $\overline{\varpi}$ is defined as in (2.12), and for convenience we have introduced the function

$$G(s) = \frac{1}{2}\left(\frac{\mathrm{e}^{-s^2}}{\sqrt{\pi}\,s} + \operatorname{erfc}(-s)\right). \tag{2.14}$$

2.4. Governing equations and boundary conditions. The governing continuum equations representing the Becker–Döring system (1.2) and (1.4) are given, respectively, by [7]

$$\frac{\partial y}{\partial t} = \big(1 - X_1(t)\big)\frac{\partial y}{\partial x} + \frac{\epsilon}{2}\big(1 + X_1(t)\big)\frac{\partial^2 y}{\partial x^2} - \epsilon\frac{\partial}{\partial x}\left(\frac{\overline{y}'}{\overline{y}}y\right), \tag{2.15a}$$

$$X_1(t) = \frac{C_b}{\nu D} - \int_0^\infty xy(x,t)\,\mathrm{d}x, \tag{2.15b}$$

where prime denotes differentiation with respect to x, and $t = \epsilon\kappa_1^+\nu\mathcal{X}_1^*\mathcal{T}$ is the appropriate dimensionless timescale. As in [7] we apply the boundary conditions

$$y(0,t) = X_1(t)^2\overline{y}(0), \tag{2.16a}$$

$$y \to 0 \quad \text{as } x \to \infty, \tag{2.16b}$$

which capture the behavior near the spike in monomer concentration and ensure we have a finite quantity of surfactant, respectively.

In this paper, we exploit the asymptotic properties of the system (2.15), (2.16) and the distributions (2.10) to elucidate the system behavior in each of the two stages of re-equilibration.

Copyright © by SIAM. Unauthorized reproduction of this article is prohibited.

3. Asymptotic analysis.

3.1. Analysis of the τ_1 process. The τ_1 process is characterized by the uniform shedding of individual monomers from aggregates to replenish the concentration of monomers. Guided by the Gaussian nature of the initial and equilibrium distributions, we seek a solution of the form

$$y(x,t) = \frac{\hat{B}(t)}{\sqrt{\epsilon}} \exp\left(-\frac{\hat{\beta}(t)}{\epsilon}\big(x-\hat{\omega}(t)\big)^2\right), \tag{3.1}$$

and impose the initial conditions

$$\hat{B}(0) = B_0, \qquad \hat{\beta}(0) = \beta, \qquad \hat{\omega}(0) = 1. \tag{3.2}$$

Substituting into (2.15a) and equating coefficients in powers of x, we obtain a system of ordinary differential equations for the coefficients in the *ansatz* (3.1), namely

$$\frac{\mathrm{d}\hat{B}}{\mathrm{d}t} = \hat{B}\big(2\beta - (1+X_1)\hat{\beta}\big), \tag{3.3a}$$

$$\frac{\mathrm{d}\hat{\beta}}{\mathrm{d}t} = 2\hat{\beta}\big(2\beta - (1+X_1)\hat{\beta}\big), \tag{3.3b}$$

$$\frac{\mathrm{d}\hat{\omega}}{\mathrm{d}t} = 2\beta\,(\overline{\omega} - \hat{\omega}) + X_1 - 1, \tag{3.3c}$$

while (2.15b) for $X_1(t)$ may be written in the form

$$X_1 = \frac{C_b}{\nu D} - \hat{B}\hat{\omega}\sqrt{\frac{\pi}{\hat{\beta}}}\,G\left(\hat{\omega}\sqrt{\hat{\beta}/\epsilon}\right), \tag{3.3d}$$

where G is defined as in (2.14). If $\hat{B}(t)$, $\hat{\beta}(t)$, $\hat{\omega}(t)$, and $X_1(t)$ satisfy (3.3), then the *ansatz* (3.1) solves the governing equations (2.15) and the far-field condition (2.16b) exactly and is exponentially close to satisfying the boundary condition (2.16a) at $x = 0$.

We notice that $\hat{B}$ and $\hat{\beta}$ decouple from the system (3.3) and may be evaluated in terms of $X_1(t)$ using the formulae

$$\hat{B}(t) = \frac{B_0}{\sqrt{\beta}}\sqrt{\hat{\beta}(t)}, \qquad \hat{\beta}(t) = \frac{2\beta \mathrm{e}^{4t}}{1 + \mathrm{e}^{4\beta t} + 4\beta\int_0^t X_1(t')\mathrm{e}^{4\beta t'}\,\mathrm{d}t'}. \tag{3.4}$$

It only remains, then, to solve the first-order differential equation (3.3c) for $\hat{\omega}(t)$, with X_1 related to $\hat{\omega}$ by

$$X_1 = \frac{C_b}{\nu D} - \frac{(C_b-1)}{\nu D}\,\frac{\hat{\omega}G\Big(\hat{\omega}\sqrt{\hat{\beta}/\epsilon}\Big)}{G\Big(\sqrt{\beta/\epsilon}\Big)}. \tag{3.5}$$

The solution (3.1) fails to satisfy the boundary condition (2.16a) by an exponentially small amount, and we infer that it is exponentially close to the true solution of the initial-boundary-value problem (2.15)–(2.16b), provided $\hat{\omega}\sqrt{\hat{\beta}}$ remains of order one. If so, then a comparable exponentially small error is incurred by using the approximation $G(s) \sim 1$ as $s \to \infty$, so that (3.5) reduces to

$$X_1(t) = \frac{C_b}{\nu D} - \frac{(C_b-1)}{\nu D}\,\hat{\omega}(t). \tag{3.6}$$

Copyright © by SIAM. Unauthorized reproduction of this article is prohibited.

It is then straightforward to solve (3.3c) and thus obtain

$$\hat{\omega}(t) = 1 - \frac{\nu D - 1 + 2\beta\nu D\,(1-\overline{\omega})}{C_b - 1 + 2\beta\nu D}\left[1 - \exp\left(-\frac{(C_b - 1 + 2\beta\nu D)}{\nu D}t\right)\right]. \tag{3.7}$$

Substitution into (3.4) and (3.6) yields simple explicit solutions also for $\hat{\beta}$, $\hat{B}$, and X_1.

As $t \to \infty$, the system approaches the equilibrium

$$\tilde{y}(x) = \frac{\tilde{B}}{\sqrt{\epsilon}} \exp\left(-\frac{\tilde{\beta}}{\epsilon}\,(x - \tilde{\omega})^2\right), \tag{3.8}$$

where

$$\tilde{B} = B_0\sqrt{\frac{2}{1+\tilde{X}_1}}, \quad \tilde{\beta} = \frac{2\beta}{1+\tilde{X}_1}, \quad \tilde{\omega} = \overline{\omega} - \frac{1-\tilde{X}_1}{2\beta}, \tag{3.9a}$$

and $\tilde{X}_1$ is given by

$$\tilde{X}_1 = \frac{C_b - 1 + 2\beta\,(C_b + \overline{\omega} - \overline{\omega}C_b)}{C_b - 1 + 2\beta\nu D}. \tag{3.9b}$$

In Figures 3.1 and 3.2, we compare the concentration profile and the monomer evolution given by the continuum model (2.15a) with those calculated using the *ansatz* (3.1) following the procedure outlined above, for the predilution distribution (2.9) with $\beta = 0.2$, $m = 100$, and C_b=10, upon a twofold dilution. We find that (3.1) provides an outstanding approximation to the evolution during the τ_1 process, deviating only by an exponentially small amount near $x = 0$, as expected, where it fails to satisfy the boundary condition. The profile assumed at the end of the τ_1 process is also captured exceptionally well by the equilibrium distribution (3.8). Similarly, the graph for X_1 predicted by this approximation is effectively indistinguishable from that provided by solving the full system (2.15a).

The results (3.9) provide simple analytic estimates for both the optimum micelle aggregation number and the monomer concentration at the stage where it becomes favorable for monomer to be replenished by total micelle breakdown, namely $n = m\tilde{\omega} \approx 89$ and $X_1 = \tilde{X}_1 = 0.965$ for these parameter values. However, we know that the system must finally reach an equilibrium in which $X_1 = 1$, which is clearly not the case for the approximate solution found above. The large-time limit (3.8) is thus a *pseudoequilibrium*, which will continue to evolve over the much longer τ_2 timescale, driven by the exponentially small discrepancy in the boundary condition (2.16a) at $x = 0$.

3.2. Analysis of the τ_2 process. As discussed in the introduction, the rate at which the τ_2 process occurs is dependent upon the concentration of aggregates in the intermediate region. When the concentration of intermediate aggregates is extremely low there is a vast separation in the two timescales of re-equilibration: rapid dissociation via stepwise monomer release followed by excruciatingly slow micelle reassembly to reach the equilibrium. To analyze the exponentially slow behavior during the τ_2 process, we must perform a metastable analysis of the system.

We note that the system (3.3a–c) admits a one-parameter family of steady solutions, corresponding to a distribution of the form

$$y_s(x;s) = \frac{B_s(s)}{\sqrt{\epsilon}}\exp\left(-\frac{\beta_s(s)}{\epsilon}\big(x - \omega_s(s)\big)^2\right), \qquad X_1 = s, \tag{3.10}$$

Copyright © by SIAM. Unauthorized reproduction of this article is prohibited.

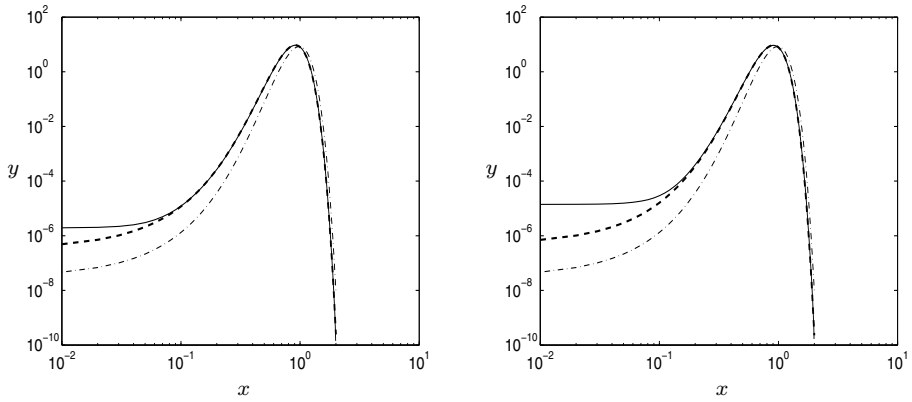

FIG. 3.1. *Comparison between the concentration profile evolutions predicted by the continuum model* (2.15a) *(solid lines) and the ansatz* (3.1) *(dashed lines) at times* (a) $t = 0.3$, (b) $t = 1$. *The predilution distribution* (2.9) *is used with parameter values* $\beta = 0.2$, $m = 100$, $C_b = 10$, *and* $D = 2$. *The dot-dash line shows the equilibrium distribution.*

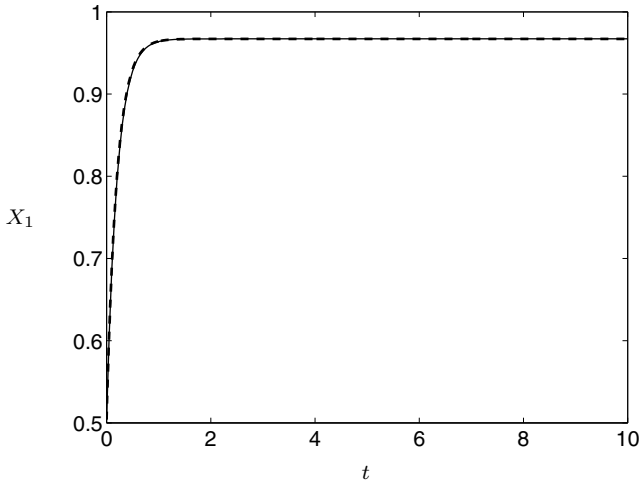

FIG. 3.2. *Comparison between the monomer concentrations predicted by the continuum model* (2.15a) *(solid lines) and using the ansatz* (3.1) *(dashed lines). The predilution distribution* (2.9) *is used with parameter values* $\beta = 0.2$, $C = 0$, $m = 100$, $C_b = 10$, *and* $D = 2$.

where

$$\beta_s(s) = \frac{2\beta}{1+s}, \qquad \omega_s(s) = \overline{\omega} - \frac{1-s}{2\beta}. \tag{3.11}$$

Equation (3.3d) gives an expression for B_s, which may be approximated by

$$B_s(s) = \frac{C_b - \nu D s}{\nu D \omega_s(s)} \sqrt{\frac{\beta_s(s)}{\pi}}, \tag{3.12}$$

with exponential accuracy.

Copyright © by SIAM. Unauthorized reproduction of this article is prohibited.

These steady solutions fail to satisfy the boundary condition (2.16a) (by an exponentially small amount), resulting in the slow evolution of y and X_1, which is given by (3.10) with $s = s(t)$. To determine this evolution we set

$$y(x,t) = y_s\big(x; s(t)\big) + \phi(x,t), \qquad X_1 = s - \xi(t), \tag{3.13}$$

where $\phi \ll y_s$, $\xi \ll 1$, and $\partial\phi/\partial t \ll \partial y_s/\partial t$. In fact, ϕ and ξ will be exponentially small. Substituting (3.13) into (2.15), linearizing and neglecting $\partial\phi/\partial t$, we obtain the equations

$$\frac{\epsilon}{2}(1+s)\frac{\partial^2\phi}{\partial x^2} + 2\beta\frac{\partial}{\partial x}\big((x-\omega_s)\phi\big) + \xi\left(\frac{\partial y_s}{\partial x} - \frac{\epsilon}{2}\frac{\partial^2 y_s}{\partial x^2}\right) = \frac{\partial y_s}{\partial s}\frac{\mathrm{d}s}{\mathrm{d}t}, \tag{3.14a}$$

$$\xi - \int_0^\infty x\phi\,\mathrm{d}x = \left(\frac{C_b}{\nu D} - s\right)\left(G\left(\omega_s\sqrt{\beta_s/\epsilon}\right) - 1\right) \tag{3.14b}$$

subject to the boundary conditions

$$\phi(0,t) = s^2\overline{y}(0) - y_s(0,s), \qquad \lim_{x\to\infty}\phi(x,t) = 0. \tag{3.15}$$

The inhomogeneous right-hand sides of (3.14) and (3.15) arise, respectively, from the slow time dependence of the metastable solution $y_s(x,s)$, the exponentially small correction to the function $G\big(\omega_s\sqrt{\beta_s/\epsilon}\big)$, and the failure of $y_s(x,s)$ to satisfy the boundary condition at $x = 0$. Since $y_s(x,s)$ is exponentially close to satisfying the homogeneous version of the original boundary-value problem (2.15), (2.16a), (2.16b) for all s, it follows that $\partial y_s/\partial s$ is exponentially close to being an eigenfunction of the perturbed problem (3.14), (3.15). This gives rise to a solvability condition that leads to a relation between the inhomogeneous terms and hence an expression for $\mathrm{d}s/\mathrm{d}t$.

The general bounded solution to (3.14a) may be written in the form

$$\phi = Ay_s - \xi\frac{\partial y_s}{\partial s} + z\frac{\mathrm{d}s}{\mathrm{d}t}, \tag{3.16}$$

where A is an integration constant and $z(x;s)$ is chosen to satisfy

$$\frac{\epsilon}{2}(1+s)\frac{\partial^2 z}{\partial x^2} + 2\beta\frac{\partial}{\partial x}\big((x-\omega_s)z\big) = \frac{\partial y_s}{\partial s}, \tag{3.17a}$$

$$z \to 0 \quad \text{as } x \to 0,\ x \to \infty. \tag{3.17b}$$

From (3.14b) and (3.15) we obtain the relations

$$Ay_s(0,s) - \xi\frac{\partial y_s}{\partial x}(0,s) = s^2\overline{y}(0) - y_s(0,s), \tag{3.18}$$

$$A\int_0^\infty xy_s\,\mathrm{d}x + \frac{\mathrm{d}s}{\mathrm{d}t}\int_0^\infty xz\,\mathrm{d}x + \left(\frac{C_b}{\nu D} - s\right)\left(G\left(\omega_s\sqrt{\beta_s/\epsilon}\right) - 1\right). \tag{3.19}$$

The term involving ξ in (3.18) is doubly exponentially small and thus negligible. Similarly, the right-hand side of (3.19) is exponentially small compared to the left-hand side, and hence $s(t)$ must satisfy the differential equation

$$\frac{\mathrm{d}s}{\mathrm{d}t}\int_0^\infty xz\,\mathrm{d}x + \left(\frac{C_b}{\nu D} - s\right)\frac{s^2\overline{y}(0) - y_s(0,s)}{y_s(0,s)} = 0. \tag{3.20}$$

Copyright © by SIAM. Unauthorized reproduction of this article is prohibited.

It only remains to calculate the integral involving the function $z(x;s)$. In Appendix B, we derive the exponentially accurate approximation

$$\int_0^\infty xz\,\mathrm{d}x \sim -\frac{\pi\omega_s}{2\beta}\frac{\mathrm{d}}{\mathrm{d}s}\left(\frac{B_s}{\sqrt{\beta_s}}\right)\mathrm{e}^{\beta_s\omega_s^2/\epsilon}\Psi\left(\omega_s\sqrt{\beta_s/\epsilon}\right), \tag{3.21}$$

where

$$\begin{aligned}\Psi(\zeta) &= \int_0^\zeta \mathrm{e}^{s^2-\zeta^2}\,\mathrm{erfc}(-s)\,\mathrm{d}s \\ &\sim \frac{1}{\sqrt{\pi}}\sum_{n=0}^{\infty}\frac{\Gamma(n+1/2)}{\zeta^{2n+1}} \quad \text{as } \zeta\to\infty,\end{aligned} \tag{3.22}$$

and (3.20) therefore reduces to

$$\frac{\mathrm{d}s}{\mathrm{d}t} = \frac{4\beta^2\nu D\omega_s^2\left(B_s\mathrm{e}^{-\beta_s\omega_s^2/\epsilon} - s^2\overline{B}\mathrm{e}^{-\beta\overline{\omega}^2/\epsilon}\right)}{\sqrt{\beta_s}\left(C_b-\nu D+2\beta\nu D\overline{\omega}\right)\Psi\left(\omega_s\sqrt{\beta_s/\epsilon}\right)}. \tag{3.23}$$

Equation (3.23) governs the exponentially slow evolution in $s(t)$, starting from the initial condition

$$s(0) = \tilde{X}_1 \tag{3.24}$$

arising from matching with the equilibrium solution (3.9) of the τ_1 problem. Equation (3.10) then gives the corresponding concentration profile.

Further simplification of (3.23) may be achieved by neglecting algebraically small terms. Provided $D < C_b$, we have $\nu \sim 1 + O(\epsilon)$ and $\overline{\omega} \sim 1 + O(\epsilon)$. We also observe in our simulations, (with relatively large bulk concentration C_b and relatively small dilution ratio D) that the monomer concentration never departs far from $X_1 = 1$. This prompts us to make the assumption that

$$s(t) = 1 - \epsilon\sigma(t), \tag{3.25}$$

where σ is treated as $O(1)$. We expect this to be valid at least during the final stages of the process where s approaches 1. Dropping terms of order ϵ, we find that (3.23) is now approximated by

$$\frac{\mathrm{d}\sigma}{\mathrm{d}t} \sim -\frac{\mathrm{e}^{-\beta/\epsilon}}{\epsilon^{3/2}}\frac{4\beta^{5/2}D\left(C_b-1\right)}{\pi\left(C_b-D+2\beta D\right)}\left(\mathrm{e}^{(1-\beta/2)\sigma}-1\right). \tag{3.26}$$

This clarifies how the timescale of evolution over the τ_2 process depends on the physical parameters in the problem. We note that the system described by (3.26) will converge towards $s = 1$ as $t \to \infty$ only if $\beta < 2$. This is a consequence of neglecting the doubly exponentially small terms in the derivation of (3.23), which will come into play when $\beta > 2$. However, since realistic surfactant distributions are unlikely to fall into this regime, we do not consider this further here.

In Figures 3.3 and 3.4 we compare, respectively, the profile distribution and evolution of X_1 over the τ_2 process predicted by the metastable dynamics analysis, (3.10)–(3.12) and (3.23) with the the full system (2.15a). The predictions are in excellent agreement with the full numerical solution. This analysis is particularly useful when,

Copyright © by SIAM. Unauthorized reproduction of this article is prohibited.

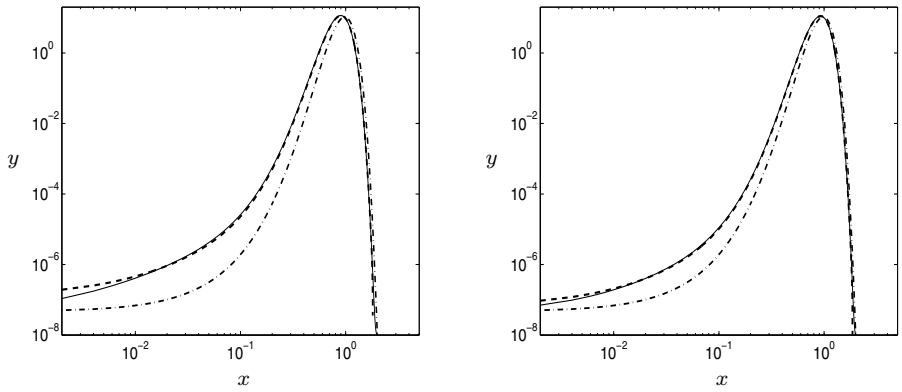

FIG. 3.3. *Comparison between the concentration profile evolutions predicted by the continuum model* (2.15a) *(solid lines) and by the metastable analysis* (3.10)–(3.12) *and* (3.23) *(dashed lines) at times* (a) $t = 10^5$, (b) $t = 10^6$. *The parameter values taken are* $\beta = 0.2$, $m = 100$, $C_b = 10$, *and* $D = 2$. *The dot-dash line shows the equilibrium distribution.*

as is the case for many realistic surfactants, the relative concentration of aggregates in the intermediate region is extremely low. As discussed above, the large separation between the timescales for the τ_1 and τ_2 processes results in the full numerical solution being computationally expensive. However, since the metastable analysis is exponentially accurate, it also provides very good agreement even when the intermediate aggregate concentration is only moderately low. Due to the exponentially long timescales over which the τ_2 process evolves, it is important to note, however, that the re-equilibration behavior for surfactants with a distribution for which C is exponentially small but nonzero in (2.8) will still be distinct from the behavior observed here when we set $C = 0$. The further simplification provided by (3.26) is also shown to provide an exceptional representation of the behavior during the τ_2 process in Figure 3.4.

4. Conclusions. In this paper, we examined the mechanism for the re-equilibration of a micellar surfactant solution following an order-one dilution. During re-equilibration, aggregates release material to replenish the concentration of monomers back to its critical value, and we adopted the usual assumption that the breakdown or assembly of surfactant aggregates occurs via stepwise monomer loss or gain, respectively. This leads to the set of coupled nonlinear ODEs known as the Becker–Döring equations. We considered a typical realistic system, in which the surfactant exists predominantly either in monomer form or as large aggregates (micelles) centred around an optimum aggregation number, with an intermediate separating region of much lower concentration.

For the majority of surfactant systems, the number of monomers that make up a micelle is large, so that the behavior may be described by a continuum model composed of a PDE governing the evolution of aggregate concentrations coupled to an integral equation for the monomer concentration. Such a system removes the complexity of tracking each species individually and vastly simplifies numerical computation, as well as allowing us to explain observations and mechanisms not elucidated by analysis of the original Becker–Döring system.

Copyright © by SIAM. Unauthorized reproduction of this article is prohibited.

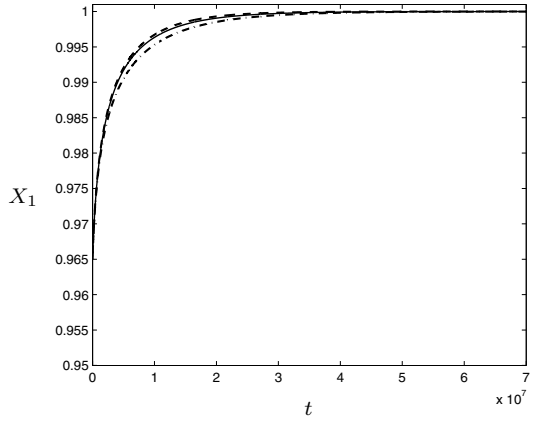

FIG. 3.4. *Comparison between the monomer evolution predicted by the continuum model* (2.15a) *(solid line), by the metastable system* (3.10)–(3.12) *and* (3.23) *(dashed line), and by* (3.26) *(dot-dashed line). The parameter values taken are* $\beta = 0.2$, $m = 100$, $C_b = 10$, *and* $D = 2$.

The re-equilibration process is characterized by two distinct stages, which are referred to as the τ_1 and τ_2 processes. In the τ_1 process, following dilution, the depleted monomer is replenished by the shedding of individual monomers from aggregates near micellar size, leading to a decrease in the dominant aggregate size. The τ_2 process is characterized by the entire breakdown of some aggregates via stepwise monomer release. Here, some of the monomers released remain in this form to replenish the monomer to the equilibrium, while the remainder associate with some of the aggregates which have not dissociated. This has the simultaneous impact of increasing the dominant aggregate size while decreasing the total concentration of surfactant contained in aggregates.

The relative timescales of the τ_1 and τ_2 processes are related to the relative concentration of aggregates in the intermediate region. For typical surfactants, this is often many orders of magnitude lower than the concentration of proper micelles, leading to well-separated timescales. This allows us to use perturbation methods to derive simplified models describing the behavior in the two distinct stages.

In the τ_1 process, the problem reduces to solving three ODEs and an integral relation. This system was explicitly solved to provide the profile evolution and was shown to capture the behavior impeccably. In addition, the analysis predicts the adoption of a pseudoequilibrium following the τ_1 process, accurately replicating the behavior observed for full system. This allows us to ascertain the time and the corresponding aggregate distribution at which it becomes favorable for monomer replenishment to occur through entire micelle breakdown via the τ_2 process.

To understand the much longer re-equilibration behavior of the τ_2 process requires a metastable analysis. Exploiting the fact that the system possesses a one-parameter family of steady solutions, we reduced the system dynamics during this process to a single ODE that determines the monomer concentration, while the aggregate distribution is selected from the family of explicit metastable solutions for each particular monomer concentration. We note that the theory presented for this stage of re-equilibration is valid only when we set $C = 0$ in the distribution (2.8) and will be distinct from the re-equilibration behavior observed during the τ_2 process when C is exponentially small but nonzero.

Copyright © by SIAM. Unauthorized reproduction of this article is prohibited.

In each of the regimes the asymptotic approximations to the behavior dramatically simplify the governing system, reducing to an exact explicit formulation for the τ_1 process, and a single ODE for the τ_2 process. The enhanced understanding of the expected behavior of typical surfactant systems provided by such simplified models is a key step forward in their optimization in practical and industrial scenarios.

Appendix A. Key results of [7]. In the preceding paper to this series, [7], the breakdown of a system of micellar aggregates in a surfactant solution following an order-one dilution is investigated. The continuum description for the micelle breakdown process that is utilized in this paper is derived from the conventional Becker–Döring equations by exploiting the largeness of the typical aggregation number of a micelle. Similarly, appropriate boundary conditions that connect the continuum aggregate distribution to the monomer concentration are derived to close the system. The typical initial distribution for a polyoxyethylene glycol alkyl ether surfactant is determined via the results of an MD simulation, and it is shown how this may be used to provide the equilibrium distribution to which the system evolves following a dilution. In equilibrium the system is shown to be composed predominantly of premicellar aggregates and a region of proper micelles close to the peak aggregation number, connected by an intermediate region containing a very low concentration of aggregates.

The resulting continuum model is solved numerically, and it is shown that the re-equilibration occurs over two distinct timescales, called the τ_1 and τ_2 processes, which is a direct result of the characteristic shape of the surfactant distribution, in particular the low concentration of intermediate aggregates.

Appendix B. Calculation of the integral (3.21). We use the substitution

$$x = \omega_s + \sqrt{\frac{\epsilon}{\beta_s}}\,\zeta \tag{B.1}$$

to rewrite (3.17) in the form

$$\frac{\mathrm{d}}{\mathrm{d}\zeta}\left(\mathrm{e}^{-\zeta^2}\frac{\mathrm{d}}{\mathrm{d}\zeta}\left(\mathrm{e}^{\zeta^2}z\right)\right) = \frac{2\mathrm{e}^{-\zeta^2}}{\sqrt{\epsilon}(1+s)\beta_s}\left(B_s' - \frac{B_s\beta_s'}{\beta_s}\zeta^2 + \frac{2B_s\sqrt{\beta_s}\omega_s'}{\sqrt{\epsilon}}\zeta\right), \tag{B.2}$$

$$z \to 0 \quad \text{as } \zeta \to -\zeta^*,\ \zeta \to \infty, \tag{B.3}$$

where

$$\zeta^* = \omega_s\sqrt{\frac{\beta_s}{\epsilon}}, \tag{B.4}$$

and prime denotes differentiation with respect to s.

The solution to (B.2) is

$$z = \frac{2}{\sqrt{\epsilon}(1+s)\beta_s}\left\{\frac{\sqrt{\pi}}{4}\left(\frac{B_s\beta_s'}{\beta_s} - 2B_s'\right)\left(\Psi(\zeta^*)\mathrm{e}^{\zeta^{*2}-\zeta^2} - \Psi(-\zeta)\right) - B_s\omega_s'\sqrt{\frac{\beta_s}{\epsilon}}\,(\zeta+\zeta^*) + \frac{B_s\beta_s'}{4\beta_s}\left(\zeta^2 - \zeta^{*2}\right)\right\}, \tag{B.5}$$

where

$$\Psi(\zeta) = \int_0^\zeta \mathrm{e}^{s^2-\zeta^2}\,\mathrm{erfc}(-s)\,\mathrm{d}s. \tag{B.6}$$

Copyright © by SIAM. Unauthorized reproduction of this article is prohibited.

Only the exponentially large term involving $\mathrm{e}^{\zeta^{*2}}$ needs to be retained when approximating

$$\begin{aligned}\int_0^\infty xz\,\mathrm{d}x &= \frac{\epsilon}{\beta_s}\int_{-\zeta^*}^\infty (\zeta+\zeta^*)\,\mathrm{d}\zeta \\ &\sim \frac{\pi\sqrt{\epsilon}}{2(1+s)\beta_s^2}\left(\frac{B_s\beta_s'}{\beta_s}-2B_s'\right)\zeta^*\Psi\left(\zeta^*\right)\mathrm{e}^{\zeta^{*2}},\end{aligned} \tag{B.7}$$

which is easily rearranged to (3.21).

Acknowledgments. IMG gratefully acknowledges helpful discussions with Dr. P. J. Dellar, Professor S. D. Howison, and Professor J. R. Ockendon.

REFERENCES

[1] E. A. G. Aniansson and S. N. Wall, *On the kinetics of step-wise micelle association*, J. Phys. Chem., 78 (1974), pp. 1024–1030.
[2] E. A. G. Aniansson and S. N. Wall, *Kinetics of step-wise micelle association and dissociation. Correction and improvement*, J. Phys. Chem., 79 (1975), pp. 857–858.
[3] E. A. G. Aniansson, S. N. Wall, M. Almgren, H. Hoffmann, I. Kielmann, W. Ulbricht, R. Zana, J. Lang, and C. Tondre, *Theory of the kinetics of micellar equilibria and quantitative interpretation of chemical relaxation studies of micellar solutions of ionic surfactants*, J. Phys. Chem., 80 (1976), pp. 905–922.
[4] R. Becker and W. Döring, *Kinetische behandlung der Keimbildung in ubersattigten dampfern*, Ann. Phys., 24 (1935), pp. 719–752.
[5] D. M. Colegate, *Structure-Kinetics Relationships in Micellar Solutions of Nonionic Surfactants*, Ph.D. thesis, Durham University, Durham, UK, 2009.
[6] J. N. B. de Moraes and W. Figueiredo, *Dynamical study of a micellar system*, Phys. Status Solidi, 187 (2001), pp. 57–62.
[7] I. M. Griffiths, C. D. Bain, C. J. W. Breward, D. M. Colegate, P. D. Howell, and S. L. Waters, *On the predictions and limitations of the Becker–Döring model for reaction kinetics in micellar surfactant solutions*, J. Coll. Int. Sci., 360 (2011), pp. 662–671.
[8] M. Jorge, *Molecular dynamics simulation of self-assembly of n-Decyltrimethylammonium Bromide micelles*, Langmuir, 24 (2008), pp. 5714–5725.
[9] J. Lang, C. Tondre, R. Zana, R. Bauer, H. Hoffmann, and W. Ulbricht, *Chemical relaxation studies of micellar equilibriums*, J. Phys. Chem., 79 (1975), pp. 276–283.
[10] G. Mohan and D. I. Kopelevich, *A multiscale model for kinetics of formation and disintegration of spherical micelles*, J. Chem. Phys., 128 (2008), 044905.
[11] M. J. Rosen, *Surfactants and Interfacial Phenomena*, John Wiley, New York, 2004.
[12] R. Nagarajan and E. Ruckenstein, *Aggregation of amphiphiles as micelles or vesicles in aqueous media*, J. Colloid Int. Sci., 71 (1979), pp. 580–604.
[13] R. Nagarajan and E. Ruckenstein, *Theory of surfactant self-assembly: A predictive molecular thermodynamic approach*, Langmuir, 7 (1991), pp. 2934–2969.
[14] S. Puvvada and D. Blankschtein, *Molecular-thermodynamic approach to predict micellization, phase behavior and phase separation of micellar solutions.* I. *Application to nonionic surfactants*, J. Chem. Phys., 92 (1990), pp. 3710–3724.
[15] M. Teubner, *Theory of ultrasonic-adsorption in micellar solutions*, J. Phys. Chem., 83 (1979), pp. 2917–2920.
[16] T. Yasunaga, K. Takeda, and S. Harada, *Kinetic study of Sodium Dodecyl Sulfate micelle dissociation by a stopped-flow method*, J. Colloid Int. Sci., 42 (1973), pp. 457–463.

Copyright © by SIAM. Unauthorized reproduction of this article is prohibited.